Ni or Co single atomic anchored conjugated microporous polymer for high-performance photocatalytic hydrogen evolution

Chen Yang,[a] Zhonghua Cheng,[a] Giorgio Divitini,[b] Cheng Qian,[a] Bo Hou,[c] Yaozu Liao*[a]

The fabrication of single atomic photocatalysts via a simple pathway is a crucial challenge to enable the efficient production of hydrogen. Herein, we demonstrate a gaseous diffusion strategy to construct single atomic photocatalysts by using the intrinsic nanopore of pyridyl-functionalized conjugated microporous polymer (PCMP) to host nickel (Ni) or cobalt (Co) atoms. Comprehensive microscopy and spectroscopy characterizations were carried out to understand the morphology and structure variations of Ni or Co single atomic anchored PCMP as photocatalysts. The experimental results show that Ni or Co present as single atoms anchoring with pyridyl nitrogen, which prominently alter the electronic structures of PCMP and delocalize the charge density of the metal atom to promote proton adsorption. The outcome of the single atomic anchoring substantially reduces the energy barrier of photocatalytic water splitting. As a result, Ni or Co single atomic photocatalysts exhibit efficient hydrogen evolution performance with a rate of 1.72 mmol g^{-1} h^{-1} (AQE=2.05% at 420 nm) under visible-light irradiation beyond pure PCMP. Moreover, the photocatalysts show excellent stability with negligible decreases in the rate of hydrogen evolution upon long-term cycling (25 h). Our findings offer a rational way for the engineering of single atomic photocatalysts for energy and environment-related applications.

Introduction

Photocatalytic water splitting is considered as a promising green route to produce hydrogen, which is one of the most critical energy sources in the future.[1] Among the developed photocatalysts, noble metal-based catalysts such as platinum, palladium, and gold are the most effective catalysts or co-catalysts for hydrogen production.[2-4] However, the cost of utilizing noble metals would limit their commercialization and mass-production due to their scarcity and high cost. Therefore, the development of cost-effective hydrogen evolution photocatalysts with high activities is of great significance to enable the hydrogen economy.

Conjugated polymers (CPs) consisting of naturally abundant elements such as C, H, and N represent emerging low-cost semiconducting materials for photocatalytic water splitting.[5-8] CPs offer a unique scope for precisely tuning their optoelectronic properties by facile molecular engineering.[9-11] Several CPs with various structures and morphologies have been developed for visible-light-driven water splitting hydrogen evolution.[12-17] As a new family of CPs, recently, conjugated microporous polymers (CMPs) with the extended π-conjugation and intrinsic nanoporosity have drawn attention particularly.[18-20] Given the distinct topological properties and functionalities of CMPs, other emerging applications such as gas uptake and separation,[21-24] energy storage,[25-27] heterogeneous catalysis,[28-30] and sensing[31] can also be envisaged. Despite extensive research over the past few years worldwide, the practical implementation of such CMPs photocatalysts is still limited by their slow charge separation and instability.[32,33] Moreover, traditional syntheses of CMPs as photocatalysts are usually involved expansive metal catalysts and energy consumption. Therefore, facile green synthesis of low-cost CMPs with suitable functionalities and optoelectronic structures for efficient visible-light-driven water splitting remains challenges. More recently, the semiconductors doping with nonprecious transition metals as single-atom catalysts (SACs) have emerged as a new frontier in photocatalysis science because SACs have maximum atom-utilization efficiency and excellent catalytic reaction activity. CMPs provide a unique platform for preparing SACs photocatalysts due to their rich nanopores, high surface area, adjustable energy gap, and tunable functionality.[34-36] Unfortunately, the examples of single-atom doped CMPs for photocatalytic hydrogen evolution applications have not been achieved yet. To achieve single-atom doped CMPs photocatalysts, various chemical routes can be potentially explored by modifying the methods applied on organic and inorganic porous materials, including photochemistry, wet impregnation, NH_3 treatment, and atomic layer deposition techniques.[37-42] However, these approaches are often energy-intensive, involving expensive equipment as well as extreme

[a] State Key Laboratory for Modification of Chemical Fibers and Polymer Materials, College of Materials Science and Engineering, Donghua University, Shanghai 201620, China
[b] Department of Materials Science and Metallurgy, University of Cambridge, 27 Charles Babbage Road, Cambridge, CB3 0FS, UK
[c] School of Physics and Astronomy, Cardiff University, Cardiff, CF24 3AA, Wales, UK
* E-mail: yzliao@dhu.edu.cn

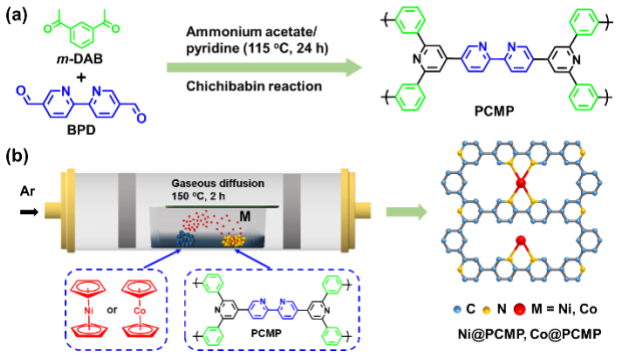

Fig. 1 Synthetic routes of (a) PCMP and (b) single atom photocatalysts i.e. Ni@PCMP, Co@PCMP.

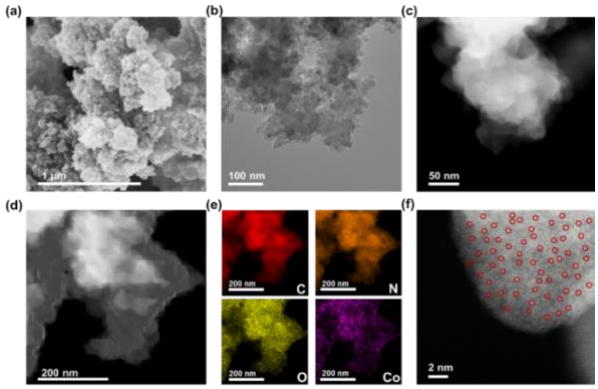

Fig. 2 (a) SEM, (b) TEM, (c) medium and (d) low-resolution AC-HAADF-STEM, (e) elemental maps, and (f) high-resolution AC-HAADF-STEM images of 30%Co@PCMP.

preparation conditions. Therefore, it is highly desirable to develop an alternative to prepare nonprecious single-atom metal-doped CMPs for photocatalytic hydrogen evolution.

In this study, we proposed a facile gas diffusion strategy to prepare novel single-atom catalysts using pyridyl-functionalized conjugated microporous polymer (PCMP) as a precursor and nickel (Ni) and cobalt (Co) as dopants for efficient photocatalytic hydrogen evolution. Firstly, PCMP is synthesized via a modified Chichibabin reaction according to the method previously reported,[43] offering a low-cost green approach to prepare conjugated microporous polymers as new photocatalysts. Then, nickelocene or cobaltocene is successfully trapped into the PCMP precursor via evaporation and adsorption. We found the active sites and band edge positions of PCMP semiconductor can be well-modulated by the content of metal dosages and metal species. Owing to the presence of isolated Co-N and pyridyl N active sites, the resultant PCMP photocatalysts with highly dispersed Co single-atom exhibit much-enhanced hydrogen evolution rate and long-term durability. Such Co single atomic anchored PCMP exhibits >200% improvements in hydrogen evolution than pure PCMP under visible light irradiation. Our findings provide a versatile route toward constructing a new class of CMPs photocatalysts with isolated single-atom metal centres for water splitting hydrogen generation.

Results and discussion

The synthetic routes to PCMP and corresponding metal (Ni or Co) anchored PCMP are shown in **Fig. 1**. By refluxing at 115 °C for 24 h, the Chichibabin reaction between 1,3-diacetylbenzene (*m*-DAB) and 2,2'-bipyridyl-5,5'-dialdehyde (BPD) in the presence of ammonium acetate and pyridine gave yellowish PCMP powder with a good yield of 80% (**Fig. 1a**). This approach provides a green avenue to synthesize PCMP, which is usually difficult to be obtained via the metal-catalyzed cross-coupling of pyridine monomers (**Table S1**).[43] The polymerization mechanism of PCMP is shown in **Fig. S1**. Verification of the structure of PCMP is achieved by Fourier transform infrared (FT-IR) and solid-state ^{13}C cross-polarization with magic angle spinning nuclear magnetic resonance (^{13}C CP/MAS NMR) spectral analyses. For comparison, the FT-IR spectra of the building block of m-DAB and BPD are provided. After the reaction, the band at ~1680 cm^{-1} assigned to the carbonyl group of m-DAB and BPD disappears in PCMP,[44] whilst the band at ~1600 cm^{-1} assigned to the pyridyl group becomes much stronger (**Fig. S2a**),[45] manifesting the successful Chichibabin coupling. The solid-state ^{13}C CP/MAS NMR spectrum of PCMP (**Fig. S2b**) exhibits four primary resonances at ~154, ~147, ~135, and ~120 ppm owing to the *ortho*-, *para*- and *meta*-substituted carbon of pyridine unit and the carbon connecting two pyridine units,[46] respectively, identifying the chemical structure of PCMP showed in **Fig. 1a**. N_2 adsorption/desorption isotherms indicate the microporosity of PCMP with a specific surface area of 324 $m^2\ g^{-1}$ and an average pore size of 0.7 nm (**Fig. S3**). Therefore, the pyridyl functionality and nanopore of PCMP offer the possibility of anchoring single atomic metals via nanoconfinement and coordination interaction. To realize the idea, a general gaseous diffusion of nickelocene or cobaltocene was applied to dope a trace amount of isolated Ni or Co active centers on PCMP support. Upon heating, nickelocene or cobaltocene powder was first sublimed into a gas phase and then diffused and trapped into PCMP support. Compared to traditional methods (**Table S1**), our strategy gave novel transition metal single atomic anchored PCMP, i.e. xM@PCMP (where x represents the dosage of nickelocene or cobaltocene metal precursors in mass related to PCMP support, M represents Ni or Co) (**Fig. 1b**).

Upon Ni or Co doping, as-prepared Ni@PCMP and Co@PCMP show decreased specific surface areas from 324 $m^2\ g^{-1}$ to 100 and 154 $m^2\ g^{-1}$, respectively (**Fig. S3a**). The inductively coupled plasma mass spectrometry (ICP-MS) analyses and full survey X-ray photoelectronic spectral (XPS) results indicate that Ni and Co elements have been successfully anchored on PCMP via the gaseous diffusion strategy (**Table S2** and **Figs. S4a,5a**). The ICP-MS results show that the concentrations of Co (0.06-0.32 wt%) presented in Co@PCMPs are lower than Ni (2.2-4.26 wt%) presented in Ni@PCMPs under the same temperature

activation. The Ni@PCMPs and Co@PCMPs show the characteristic FT-IR spectra of pure PCMP (**Fig. S6a,c**). X-ray diffraction (XRD) patterns confirm amorphous structures of Ni@PCMPs and Co@PCMPs (**Fig. S6b,d**). Scanning electron microscope (SEM) and transmission electron microscope (TEM) images show that the agglomerates of PCMP consist of nanoparticles with diameters of ~70 nm (**Fig. S7**). Upon doping with either Ni or Co, the nanoparticles of PCMP became more aggregated and tended to form sheet-like morphologies **(Fig. 2a,b** and **Fig. S8a,b**). The medium-resolution aberration-corrected high-angle annular dark-field scanning transmission electron microscopy (AC-HAADF-STEM) image of a typical 30%Co@PCMP displays no Co species particles (**Fig. 2c**), suggesting that Co atoms are homogeneously dispersed and coordinated with N atoms of PCMP. Elemental mapping images of 30%Co@PCMP further reveal that Co elements are highly dispersed and well distributed in a polymeric framework (**Fig. 2d,e**). The high-resolution AC-HAADF-STEM image in **Fig. 2f** presents many bright dots spread over a large area, with no clusters or small particles being observed, signifying that Co is dispersed at the atomic scale.[47] Although Ni elements are also homogenously distributed in PCMP, both Ni single atoms and Ni nanoclusters clearly present (**Fig. S8c-f**). The results indicate that Co single atoms are easier stabilized by PCMP compared to Ni owing to the higher diffusion barriers, electronegativity and low surface free energy.[48,49]

The C1s, N1s, Ni2p and Co2p core-level XPS spectra were also obtained to analyze the structure of xM@PCMP. The C1s core-level XPS spectra confirm the formation of the desired structures (**Fig. 1b)**, displaying three peaks at ~284.6, ~285.4 and ~287.1 eV, which can be attributed to aryl -C=C-, -C=N- and -C=O- bonds (**Fig. 3a**), respectively. The PCMP exhibits a single N1s XPS peak at ~398.6 eV owing to pyridinic (**Fig. 3b**).[50,51] Besides, 30%Ni@PCMP and 30%Co@PCMP display two additional peaks at 399.5 and 399.2 eV due to Ni-N and Co-N bonds, respectively, indicating Ni-N and Co-N coordination.[41-53] The 30%Ni@PCMP shows Ni2p XPS peak splits into two satellite $Ni2p_{1/2}$ and $Ni2p_{3/2}$ spin orbits due to oxidized Ni (**Fig. 3c**).[54,55] The 30%Co@PCMP displays that Co2p XPS peak splits into two $Co2p_{1/2}$ and $Co2p_{3/2}$ spin orbits at 781.0 and 796.2 eV (**Fig. 3d**), implying the formation of Co-N.[56,57] By altering the dosage of Ni and Co metals, the obtained samples also present similar bond information (**Figs. S4,5**). Such Ni-N and Co-N coordination are beneficial to the hydrogen production performance of PCMP since Ni and Co oxidations are capturing sites to accept photons, which separating the electron-hole pairs easier.[58,59]

To gain more insights into the relationship between the structure and photocatalytic activity, the ultraviolet-visible (UV-vis) diffuse reflectance spectra were examined to investigate the band gap (E_g) of Ni@PCMPs and Co@PCMPs (**Fig. S9**). It can be seen from **Fig. 4a**, compared with PCMP (~500 nm) and 30%Co@PCMP (~500 nm), 30%Ni@PCMP (600 nm-700 nm) have a wider fundamental absorption range. According to the Kubelka-Munk function,[60] the E_g is determined from the absorption spectra using the equation as follows:

$$\alpha hv = A\left(hv - E_g\right)^{n/2} \quad (1)$$

where α, h, v, E_g, and A represents optical absorption coefficient, Planck constant, frequency of the incident photon, band gap and a constant depending on electron-hole mobility, respectively. The value of n is 1. The values of α and A can be obtained according to the following equations:

$$\alpha = A(1 - R)^2/2R \quad (2)$$

$$A = -\lg(R) \quad (3)$$

where R is the reflectance. According to equation (1), (2) and (3), the E_g values of as-synthesized samples was calculated. The results demonstrate that the E_g of PCMP, 30%Ni@PCMP and 30%Co@PCMP are 2.63, 2.53, and 2.54 eV, respectively (**Fig. 4b** and **Table 1**), indicating that all catalysts have enough band gap for photocatalytic water

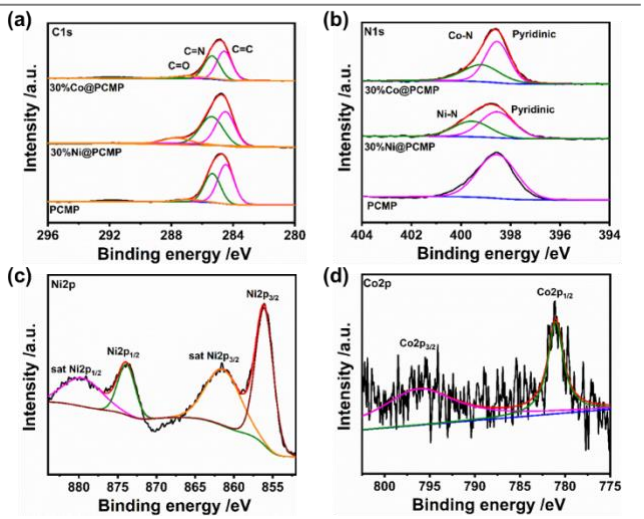

Fig. 3 (a) C1s and (b) N1s, (c) Ni2p, and (d) Co2p core-level XPS spectra of PCMP, 30%Ni@PCMP, and 30%Co@PCMP.

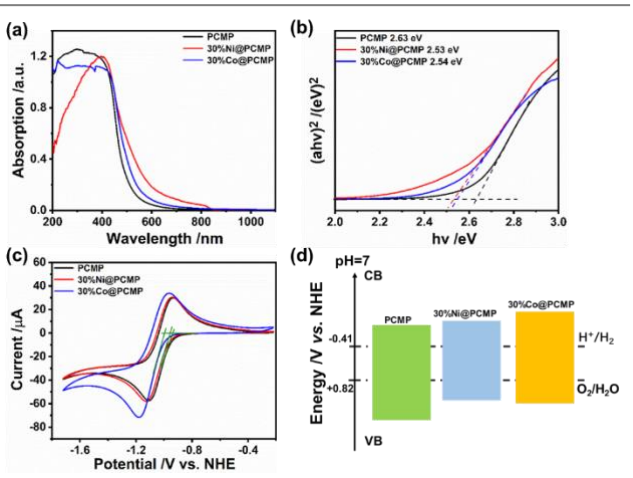

Fig. 4 (a) UV-vis spectra, (b) Tauc plots, (c) CV curves, and (d) schematic illustration of the electronic band structures of PCMP, 30%Ni@PCMP and 30%Co@PCMP.

splitting.[61-63] Meanwhile, the E_g values of Ni or Co single atomic anchored PCMP can be regulated by the dosage of

Table 1 Metal content, band gaps (E_g) and band positions (E_{CB} and E_{VB}) of PCMP, 30%Ni@PCMP and 30%Co@PCMP.

Sample	Ni (wt%)	Co (wt%)	E_g (eV)	E_{CB} (eV)	E_{VB} (eV)	H_2 evolution rate (mmol g^{-1} h^{-1})
PCMP	-	-	2.63	-0.93	1.7	0.83
30%Ni@PCMP	2.97	-	2.53	-0.95	1.58	0.97
30%Co@PCMP	-	0.14	2.54	-1.00	1.54	1.72

decrease and then increase with the Ni and Co dosage rising from 10% to 50% (**Tables S3,4**), respectively. Both Ni@PCMPs and Co@PCMPs exhibit the narrowest E_g when 30% of metal dosage is applied. Upon single atomic anchoring, Ni or Co atoms tend to be embedded into the PCMP network and act as bridges to facilitate the charge carrier transfer owing to the effects of conduction band offset, explaining both 30%Ni@PCMP and 30%Co@PCMP show reduced band gaps compared with pure PCMP. It is widely recognized that the reduced band gaps are beneficial for the light absorption ability of photocatalysts, which is crucial for improving photocatalytic performance.

Cyclic voltammetry (CV) measurements were further conducted to identify the conduction band (CB) positions of the Ni@PCMP and Co@PCMP samples (**Fig. 4c,d** and **Figs. S10,11**). The valence band (VB) positions are derived by adding the E_g to the E_{CB} value.[64] In **Table 1**, the different E_{CB} and E_{VB} energy levels of PCMP, 30%Ni@PCMP and 30%Co@PCMP are presented, where E_{CB} positions are much higher than the potentials of H^+/H_2 (-0.41 eV, pH = 7). Since the redox potentials for proton reduction and water oxidation at pH = 7 are -0.41 and +0.82 eV *versus* the NHE level, the electronic band structures of the three samples are well-positioned for visible-light-driven hydrogen generation. It is found that the E_{CB} values of the samples follow a sequence: 30%Co@PCMP (more negative than -1.00 eV) > 30%Ni@PCMP (-0.95 eV) > PCMP (-0.93 eV). With increasing the dosage of metals from 0 to 50%, 30%Ni@PCMP and 30%Co@PCMP exhibit the most negative E_{CB} positions, respectively. The results indicate that 30%Co@PCMP has the strongest reduction ability.[65]

The hydrogen evolution experiments were performed using photocatalyst powders suspended in water under visible light irradiation (λ > 420 nm, Xe lamp), where triethanolamine (TEOA) as the hole sacrificial agent and Pt (3 wt%) as the co-catalyst were added.[66-69] The hydrogen evolution performance quantitively characterized by gas chromatography (GC) is shown in **Fig. 5a** and **Fig. S12**. Both Ni@PCMPs and Co@PCMPs exhibit the highest hydrogen evolution rates when 30% of metal dosage is used. Encouragingly, the photocatalytic hydrogen evolution activity of 30%Co@PCMP was enhanced more than 200% compared with pure PCMP. 30%Co@PCMP exhibits much higher hydrogen evolution performance compared to PCMP (1.72 vs 0.84 mmol g^{-1} h^{-1}) and 30%Ni@PCMP (1.72 vs 0.97 mmol g^{-1} h^{-1}). This hydrogen evolution rate is higher than most recently reported values for conjugated polymers (such as PCMPs, CTFs, CTPs, and IEPs) and metal-modified polymers (such as PCP1e-PCP4e, P1s, Cd-TBAPy and DETPPs) (**Table S5**). Compared to PCMP and 30%Ni@PCMP (0.77% and 1.19%), much enhanced apparent quantum efficiency (AQE, measured at 420 nm) found on 30%Co@PCMP (2.05%) explains the excellent hydrogen evolution performance. Meanwhile, considering that the referenced materials were synthesized via the palladium-catalyzed coupling reaction and harsh reaction conditions (high temperature, high pressure, long time and complicated equipment etc.), our protocol provides a promising green route to prepare low-cost photocatalysts for water splitting. For comparison, the photocatalytic hydrogen evolution activity of PCMP, 30%Ni@PCMP and 30%Co@PCMP without Pt are also provided (**Figs. S13,14**). The results demonstrate that the hydrogen generation rate of PCMP, 30%Ni@PCMP and 30%Co@PCMP are 0, 196.52, and 505.27 μmol g^{-1} h^{-1}, respectively, indicating that catalytic activity is derived from Ni or Co single atoms, especially Co. Considering that the suitable electronic band structures of PCMP, 30%Ni@PCMP and 30%Co@PCMP for water oxidation, photocatalytic oxygen evolution was further evaluated. As shown in Fig. S15, shows much higher oxygen evolution performance compared to PCMP (48 vs 15 μmol g^{-1} h^{-1}) and 30%Ni@PCMP (48 vs 27 μmol g^{-1} h^{-1}).

Photoluminescence (PL) and time-resolved photoluminescence decay spectra were examined to compare the charge separation efficiency among PCMP, Ni@PCMPs and Co@PCMPs. A strong PL emission peak located at approximately 523 nm is observed for PCMP (**Fig. 5b**), which may be attributed to the recombination radiation of photoinduced charge carriers and excitons.[70] Although the position of the PL emission peaks of Ni@PCMPs (~537 nm) and Co@PCMPs (~541 nm) is close to that of PCMP (~523 nm), which intensity is drastically reduced (**Fig. S15**). Especially, the PL emission intensity of 30%Ni@PCMP and 30%Co@PCMP have been significantly reduced. Much higher charge separation efficiency is observed on 30%Co@PCMP than the values observed on 30%Ni@PCMP and PCMP (**Fig. 5b**), which is also confirmed by the time-resolved PL decay spectra (**Fig. 5c**). It is found that the average lifetime of PCMP (1.13 ns) increases to 1.21 ns and 1.52 ns for 30%Ni@PCMP and 30%Co@PCMP, respectively. The longer lifetime is believed to be beneficial for photocarrier transfer,[71] explaining the improved hydrogen evolution observed on Co@PCMP. The time courses of photocurrent of the samples indicate that the most substantial photocurrent response is found on 30%Co@PCMP (**Fig. 5d**). The obtained Nyquist plots **(Fig. S16)** show that the diameters of the semicircles for 30%Ni@PCMP and 30%Co@PCMP are smaller than that of PCMP, particularly 30%Co@PCMP, suggesting that the single atomic metals contribute to photo-generated electron-hole pair separation and efficient charge transfer better.[72] The results signify that 30%Co@PCMP is much more sensitive to visible light irradiation and effectively promotes the separation and transfer of photo-generated electron-hole pairs, consistent with the better photocatalytic activity observed.

To further evaluate the hydrogen evolution performance, the stability of PCMP, 30%Ni@PCMP and 30%Co@PCMP were further investigated upon long-term irradiation. As can be seen in **Fig. 6a**, steady photocatalytic hydrogen evolution is observed in five consecutive runs over a total of 25 h. The SEM images show that the morphology of PCMP, 30%Ni@PCMP and 30%Co@PCMP keep the original appearance upon 25 h irradiation (**Fig. S17**). XRD patterns confirm that PCMP, 30%Ni@PCMP and 30%Co@PCMP are almost unchanged (**Fig. S18**). The FT-IR spectral analyses show that both the functional groups and intrinsic conjugated skeletons of polymers maintain in the same state upon 25 h irradiation (**Fig. 6b-d**), verifying the excellent recyclability and photocorrosion-resistance of PCMP, 30%Ni@PCMP and 30%Co@PCMP. The stability was further confirmed by XPS spectral analyses (**Fig. 7** and **Figs. S19,20**). Upon 25 h of irradiation, the main XPS peaks of all the photocatalysts

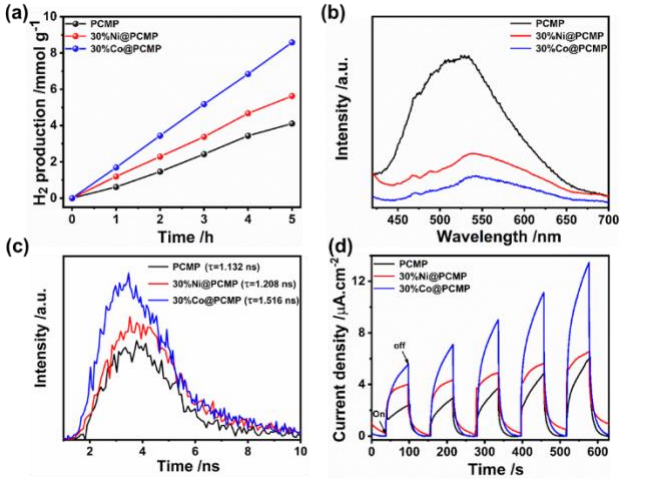

Fig. 5 (a) Time courses of hydrogen production, (b) photoluminescence emission spectra (λ_{ex}=380 nm), (c) time-resolved photoluminescence decay spectra (λ_{ex}=337 nm) and (d) time courses of photocurrent of PCMP, 30%Ni@PCMP and 30%Co@PCMP.

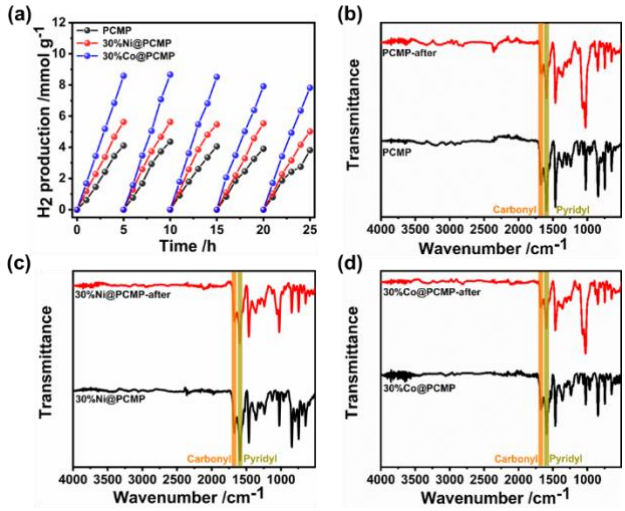

Fig. 6 Photocatalytic stability tests: (a) time courses of hydrogen production and (b-d) FT-IR spectra of PCMP, 30%Ni@PCMP, and 30%Co@PCMP upon 25 h cycling.

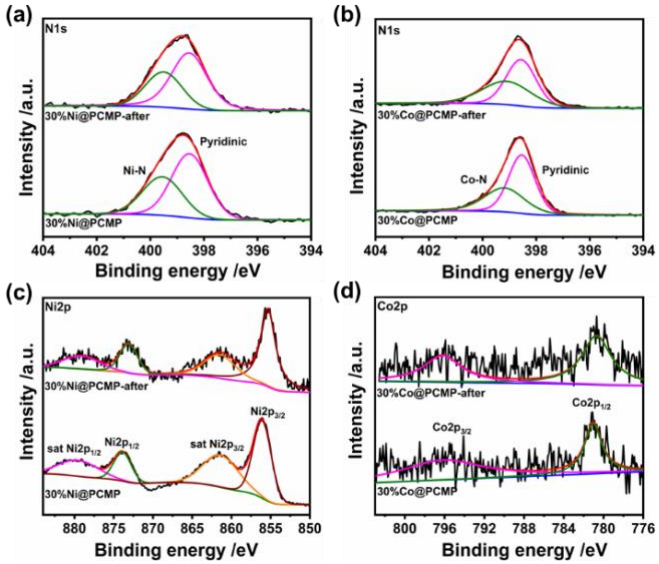

Fig. 7 Core-level XPS spectra of PCMP, 30%Ni@PCMP, and 30%Co@PCMP upon 25 h cycling.

show negligible changes. The C1s, N1s, Ni2p and Co2p core-level XPS spectra also display that the peaks of -C=C-, -C=N-, -C=O-, Ni-N, and Co-N bonds keep the original position upon irradiation, further testifying to the excellent stability of as-prepared photocatalysts. To testify the universality of the strategy, 30%Fe@PCMP was also prepared using ferrocene as a precursor. The SEM, TEM and elemental mapping observations (Fig. S22) indicate that Fe element was successfully anchored on PCMP. However, 30%Fe@PCMP exhibits a slight increase in hydrogen evolution performance compared to PCMP (0.87 vs 0.84 mmol $g^{-1}h^{-1}$) (Fig. S23). This may be related to the instability, diffusion barriers and electronegativity of the Fe element.[73]

Based on the above results and discussion, a possible mechanism of photocatalytic hydrogen evolution for xM@PCMP is proposed in **Fig. S21**. Photogenerated electrons (e^-) jump to the E_{CB} level and holes (h^+) at the E_{VB} level. The electrons are further transferred to the surface of the PCMP for hydrogen evolution, and the sacrificial agent consumes the holes. A significant increase of the photocatalytic hydrogen evolution for Ni@PCMPs or Co@PCMPs can be explained as follows: (1) the Ni or Co single-atom content modulates the energy band position, effectively promotes the separation and transfer efficiency of photo-generated carriers; (2) the interaction between Ni and N or Co and N atoms enhances the electron transfer, changing the electronic configuration and increasing the active sites. Overall, the enhanced photocatalytic activity observed in 30%Co@PCMP can be attributed to the improved negative redox potential, surface-active sites, charge separation efficiency, photocarrier transfer, and photosensitivity.

Conclusions

In summary, a gaseous diffusion strategy has been successfully demonstrated for the synthesis of Ni or Co single-atom anchored pyridyl-functionalized conjugated microporous polymer (PCMP). The synthetic route can be conducted under a mediate temperature (150 °C) in a relatively short period (2 h). The as-prepared Ni@PCMPs and Co@PCMPs photocatalysts possess suitable electronic structures for visible-light-driven hydrogen evolution activity. Especially, 30%Co@PCMP exhibited the highest photocatalytic H_2 evolution activity, and the steady photocatalytic hydrogen evolution rate reaches up to 1.72 mmol (g^{-1} h^{-1}), which is 200% times higher than pure PCMP. We believe that this work could open a versatile and facile route for designing highly efficient CMPs anchor single-atom photocatalysts by selecting suitable metals and content.

Author Contributions

Y. Liao initiated and supervised the project. C. Yang designed and performed the experiments, analyzed the data, prepared all illustrations. Z. Cheng, G. Divitini, C. Qian and B. Hou performed the SEM, TEM, STEM measurements and helped the data analyses. All the authors wrote the manuscript and have given approval to the final version of the manuscript.

Conflicts of interest

The authors declare no competing financial interest.

Acknowledgements

This work was supported by the National Natural Science Foundation of China (52073046, 51873036 and 51673039), the Shanghai Shuguang Program (19SG28), the Natural Science Foundation of Shanghai (19ZR1470900). We furthermore acknowledge the support from the International Joint Laboratory for Advanced Fiber and Low-Dimension Materials (18520750400).

Notes and references

1 C. F. Shih, T. Zhang, J. Li and C. Bai, *Joule*, 2018, **2**, 1-25.
2 H. Wei, H. Wu, K. Huang, B. Ge, J. Ma, J. Lang, D. Zu, M. Lei, Y. Yao, W. Guo and H. Wu, *Chem. Sci.*, 2019, **10**, 2830-2836.
3 W. Zhao, Y. Jiao, J. Li, L. Wu, A. Xie and W. Dong, *J. Catal.*, 2019, **378**, 42-50.
4 Y. K. Kim and H. Park, *Energy Environ. Sci.*, 2011, **4**, 685-694.
5 C. Han, P. Dong, H. Tang, P. Zheng, C. Zhang, F. Wang, F. Huang and J. Jiang, *Chem. Sci.*, 2021, **12**, 1796-1802.
6 M. Sachs, H. Cha, J. Kosco, C. M. Aitchison, L. Francas, S. Corby, C. Chiang, A. A. Wilson, R. Godin, A. Fahey-Williams, A. I. Cooper, R. S. Sprick, I. McCulloch and J. R. Durrant, *J. Am. Chem. Soc.*, 2021, **143**, 524-524.
7 H. Yang, H. Amari, L. Liu, C. Zhao, H. Gao, A. He, N. D. Browning, M. A. Little, R. S. Sprick and A. I. Cooper, *Nanoscale*, 2020, **12**, 24488-24494.
8 Y. Zang, R. Wang, P. Shao, X. Feng, S. Wang, S. Zang and T. C. W. Mak, *J. Mater. Chem. A.*, 2020, **8**, 25094-25100.
9 H. Sirringhaus, *Science*, 1998, **280**, 1741-1744.
10 L. Wang, Y. Zhang, L. Chen, H. Xu and Y. Xiong, *Adv. Mater.*, 2018, **30**, 1801955-1801955.
11 C. Yang, B. C. Ma, L. Zhang, S. Lin, S. Ghasimi, K. Landfester, K. A. I. Zhang and X. Wang, *Angew. Chem., Int. Ed.*, 2016, **55**, 9202-9206.
12 G. Li, Z. Xie, Q. Wang, X. Chen, Y. Zhang and X. Wang, *Chem-Eur. J.*, 2021, **27**, 939-943.

13 F. Wang, W. Lei, X. Pan and Z. Ye, *Nanotechnology*, 2020, **31**, 475406.
14 J. Xiao, X. Liu, L. Pan, C. Shi, X. Zhang and J. Zuo, *ACS Catal.*, 2020, **10**,12256-12283.
15 Q. Yang, M. Luo, K. Liu, H. Cao and H. Yan, *Appl. Catal. B Environ.*, 2020, **276**, 119174.
16 J. Xu, C. Yang, S. Bi, W. Wang, Y. He, D. Wu, Q. Liang, X. Wang and F. Zhang, *Angew. Chem. Int. Ed.*, 2020, **59**, 23845-23853.
17 H. Ye, Z. Wang, Z. Yang, S. Zhang, X. Gong and J. Hua, *J. Mater. Chem. A.*, 2020, **8**, 20062-20071.
18 N. B. Mckeown and P. M. Budd, *Macromolecules*, 2010, **43**, 5163-5176.
19 J. M. Lee and A. I. Cooper, *Chem. Rev.*, 2020, **120**, 2171-2214.
20 G. Zhang, W. Ou, J. Wang, Y. Xu, D. Xu, T. Sun, S. Xiao, M. Wang, H. Li, W. Chen and C. Su, *Appl. Catal. B Environ.*, 2019, **245**, 114-121.
21 X. Hu, H. Wang, C. F. J. Faul, J. Wen, Y. Wei, M. Zhu and Y. Liao, *Chem. Eng. J.*, 2020, **382**, 122998.
22 Z. Cheng, Z. Dai, J. Li, H. Wang, M. Huang, X. Li and Y. Liao, *Chem. Eng. J.*, 2019, **357**, 776-786.
23 Y. Liao, Z. Cheng, W. Zuo, A. Thomas and C. F. J. Faul, *ACS Appl. Mater. Interfaces*, 2017, **9**, 38390-38400.
24 Y. Liao, J. Weber, B. M. Mills, Z. Ren and C. F. J. Faul, *Macromolecules*, 2016, **49**, 6322-6333.
25 M. Zhang, T. Zhao, J. Dou, Z. Xu, W. Zhang, X. Chen, X. Wang and B. Zhou, *ChemElectroChem*, 2019, **6**, 5946-5950.
26 Y. Li, W. Li, Z. Cheng, Y. He, H. Li, H. Li and Y. Liao, *ChemNanoMat*, 2019, **6**, 58-63.
27 H. Wang, Z. Cheng, Y. Liao, J. Li, J. Weber, A. Thoams and C. F. J. Faul, *Chem. Mater.*, 2017, **29**, 4885-4893.
28 L. Sekerová, P. Březinová, T. T. Do, E. Vyskoclilova, J. Krupka, L. Cerveny, L. Havelkova, B. Bashta and J. Sedlacek, *ChemCatChem*, 2019, **12**, 1075-1084.
29 X. Wang, L. Chen, S. Y. Chong, M. A. Little, Y. Z. Wu, W. H. Zhu, R. Clowes, Y. Yan, M. A. Zwijnenburg, R. S. Sprick and A. I. Cooper, *Nat. Chem.*, 2018, **10**, 1180-1189.
30 L. Chen, Y. Yang and D. Jiang, *J. Am. Chem. Soc.*, 2010, **132**, 9138-9143.
31 X. Liu, Y. Xu and D. Jiang, *J. Am. Chem. Soc.*, 2012, **134**, 8738-8741.
32 R. S. Sprick, J. X. Jiang, B. Bonillo, S. J. Ren, T. Ratvijitvech, P. Gui, M. A. Zwijnenburg, D. J. Adams and A. I. Cooper, *J. Am. Chem. Soc.*, 2015, **137**, 3265-3270.
33 X. Wang, X. Zhao, W. Dong, X. Zhang, Y. Xiang, Q. Huang and H. Chen, *J. Mater. Chem. A*, 2019, **7**, 16277-16284.
34 A. Pimachev, R. D. Nielsen and Y. Dahnovsky, *Chem. Phys*., 2020, **26**, 14480-14488.
35 X. Zhang, H. Liu, P. An, Y. Shi, J. Han, Z. Yang, C. Long, J. Guo, S. Zhao, K. Zhao, H. Yin, L. Zheng, B. Zhang, X. Liu, L. Zhang, G. Li and Z. Tang, *Sci. Adv.*, 2020, **6**, 24824.
36 H. Wang, B. Hou, Y. Yang, Q. Chen, M. Zhu, A. Thoams and Y. Liao, *Small*, 2018, **14**, 1803232.
37 Z. Qian and K. A. I. Zhang, *Sol. RRL*, 2021, **5**, 2000489.
38 Q. Zhao, J. Sun, S. Li, C. Huang, W. Yao, W. Chen, T Zeng, Q Wu and Q. Xu, *ACS Catal.*, 2018, **8**, 11863-11874.
39 L. Zeng, C. Dai, B. Liu and C. Xue, *J. Mater. Chem. A.*, 2019, **7**, 24217-24221.
40 Y. Cao, S. Chen, Q. Luo, H. Yan, Y. Lin, W. Liu, L. Cao, J. Lu, J. Yang, J, T. Yao and S. Wei, *Angew. Chem. Int. Ed.*, 2017, **56**, 12191-12196.
41 M. Piernavieja-Hermida, Z. Lu, A. White, K. B. Low, T. Wu, J. F. Elam, Z. Wu and Y. Lei, *Nanoscale*, 2016, **8**, 15348-15356.
42 T. He, S. Chen, B. Ni, Y. Gong, Z. Wu, L. Song, L. Gu, W. Hu and X. Wang, *Angew. Chem. Int. Ed.*, 2018, **57**, 3493-3498.
43 Z. Cheng, L. Wang, Y. He, X. Chen, X. Wu, H. Xu, Y. Liao and M. Zhu, *Polym. Chem.*, 2020, **11**, 3393-3397.
44 L. Zou, D. Feng, T. F. Liu, Y. P. Chen, S. Fordham, S. Yuan, J. Tian and H. C. Zhou, *Chem. Commun.*, 2015, **51**, 4005-4008.
45 H. Cao, H. Huang, Z. Chen, B. Karadeniz, J. Lv and R. Cao, *ACS Appl. Mater. Interfaces*, 2017, **9**, 5231-5236.
46 Y. He, Z. Cheng, H. Zuo, C. Yan and Y. Liao, *ChemElectroChem*, 2020, **7**, 959-966.
47 Y. Xiong, W. Sun, P. Xin, W. Chen, X. Zheng, W. Yan, L. Zheng, J. Dong, J. Zhang, D. Wang and Y. Li, *Adv. Mater.*, 2020, **32**, 2000896.
48 Y. Huang, C. An, Q. Zhang, L. Zang, H. Shao, Y. Liu, Y. Zhang, H. Yuan, C. Wang and Y. Wang, *Nano Energy*, 2021, **80**, 105535.
49 J. Huang, C. Zhou, Z. Chu, X. Liu and X. Duan, *Phys. Chem. Chem. Phys.*, 2021, **23**, 1868-1873.
50 Z. Sheng, L. Shao, J. Chen, W. Bao, F. Wang and X. Xia, *ACS Nano*, 2011, **5**, 4350-4358.
51 A. Maetz, L. Delmotte, G. Moussa, J. Dentzer, S. Knopf and C. M. Ghimbeu, *Green Chem.*, 2017, **19**, 2266-2274.
52 X. Ning, Y. Sun, H. Fu, X. Qu, Z. Xu and S. Zheng, *Chemosphere*, 2020, **241**, 124978.
53 F. Mao, P. F. Liu, P. Yang, J. Gu and H. Yang, *Chem. Commun.*, 2020, **56**, 7495-7498.
54 Y. Zhou, D. Lin, X. Ye and M. Zhu, *J. Alloys Compd.*, 2020, **839**, 155691.
55 L. Li, J. Xu and B. Su, *Appl. Surf. Sci.*, 2020, **524**, 146154.
56 H. Gong, X. Hao, H. Li and Z. Jin, *J. Colloid Interface Sci.*, 2021, **585**, 217-228.

57 Q. Zhao, W. Yao, C. Huang, Q. Wu and Q. Xu, *ACS Appl. Mater. Interfaces*, 2017, **9**, 42734-42741.
58 Y. Xing, J. Ku, W. Fu, L. Wang and H. Chen, *Chem. Eng. J.*, 2020, **395**, 125149.
59 X. Li, H. Zhang, Y. Liu, X. Duan and S. Wang, *Chem. Eng. J.*, 2020, **390**, 124634.
60 P. Sivakarthik, V. Thangara and M. Parthibavarman, *J. Mater. Sci.: Mater. Electron.*, 2017, **28**, 5990-5996.
61 L. Fang, X. Wang, Y. Li, P. Liu, Y. Wang, H. Zeng and H. Yang, *Appl. Catal., B*, 2017, **200**, 578-584.
62 L. Li, Z. Deng, L. Yu, Z Lin, W. Wang and G. Yang, *Nano Energy*, 2016, **27**, 103-113.
63 Q. Xiang, J. Yu and M. Jaroniec, *Nanoscale*, 2011, **3**, 3670-3678.
64 B. Hou, D. Parker, G. P. Kissling, J. A. Jones, D. Cherns and D. J. Fermín, *J. Phys. Chem. C*, 2013, **117**, 6814-6820.
65 J. Wang, P. Guo, M. Dou, J. Wang, Y. Cheng, P. Jonsson and Z. Zhao, *RSC Adv.*, 2014, **4**, 51008-51015.
66 Q. Shang, N. Liu, D. You, D. Q. Cheng, G. Liao and Z. Pan, *J. Mater. Chem. C*, 2021, **9**, 238-248.
67 G. Shu, Y. Li, W. Zhuang, J. Jiang and F. Wang, *Appl. Catal. B Environ.*, 2019, **261**, 118230.
68 Y. Wang, C. Zheng, M. Liu, W. Wei, J. Gao, Y. Zhang and P. Deng, *Chem. Commun.*, 2021, **57**, 3857-3860.
69 L. Luo, Z. Gong, J. Ma, K. Wang, H. Zhu, K. Li, L. Xiong, X. Guo and J. Tang, *Appl. Catal. B Environ*, 2021, **284**, 119742.
70 J. Li, H. Huang, P. Liu, X. Song, D. Mei, Y. Tang, X. Wang and C. Zhong, *J. Catal.*, 2019, **375**, 351-360.
71 W. Lin, M. H. Elsayed, J. Jayakumar, L. Ting, C. Chang, M. E. Ahmed, W. Wang, C. Chung, C. Lu and H. Chou, *Int. J. Hydrogen Energy*, 2020, **45**, 32072-32081.
72 J. Xie, C. Wang, N Chen, W. Chen, J. Xu, P. Bai, B. Liu, L. Zhang and H. Wang, H, *J. Mater. Chem. C*, 2021, **9**, 4378.
73 Y. Huang, C. An, Q. Zhang, L. Zhang, H. Shao, Y. Liu, Y. Zhang, H. Yuan, C. Wang, Y. Wang, *Nano Energy*, 2021, **80**, 105535